Electronic Supplementary Material (ESI) for Journal of Materials Chemistry A.

All-solid-state, light-weight, flexible asymmetric supercapacitor based on cabbage-like $ZnCo_2O_4$ and porous VN nanowires electrode materials

Jingxin Zhao[a,b], Chaowei Li[b], Qichong Zhang[b], Jun Zhang[b], Xiaona Wang[b], Ziyin Lin[b], Juanjuan Wang[a], Conghua Lu[a*], Ching-ping Wong[c], Yagang Yao[b*]

[a] *School of Materials Science and Engineering, Tianjin University, Tianjin, 300072, P. R. China*

[b] *Division of Advanced Nanomaterials, Key Laboratory of Nanodevices and Applications, CAS Center for Excellence in Nanoscience, Suzhou Institute of Nano-tech and Nano-bionics, Chinese Academy of Sciences, Suzhou 215123, P. R. China*

[c] *School of Materials Science and Engineering, Georgia Institute of Technology, 771 Ferst Drive, Atlanta 30332, USA*

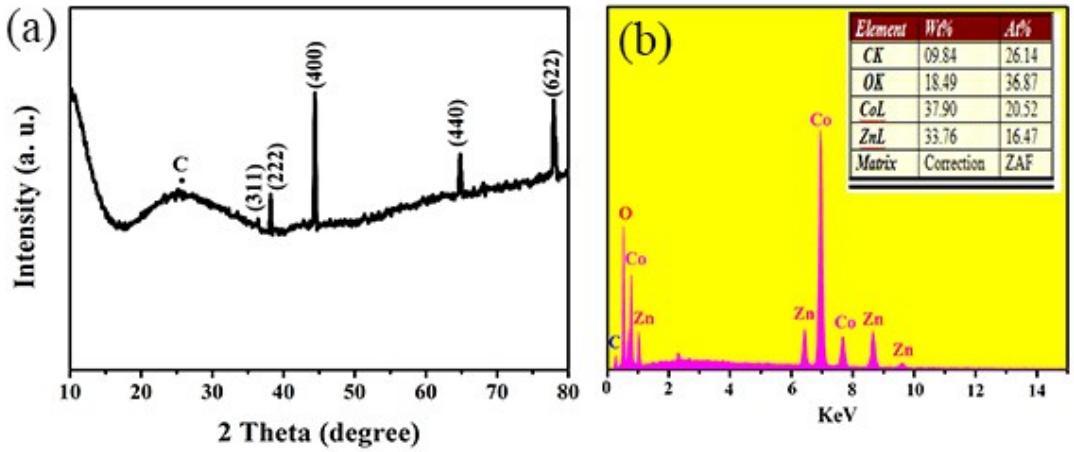

Fig. S1 (a) XRD pattern, and (b) EDS of VN nanowires.

* Corresponding author. E-mail: ygyao2013@sinano.ac.cn

* Corresponding author. E-mail: chlu@tju.edu.cn

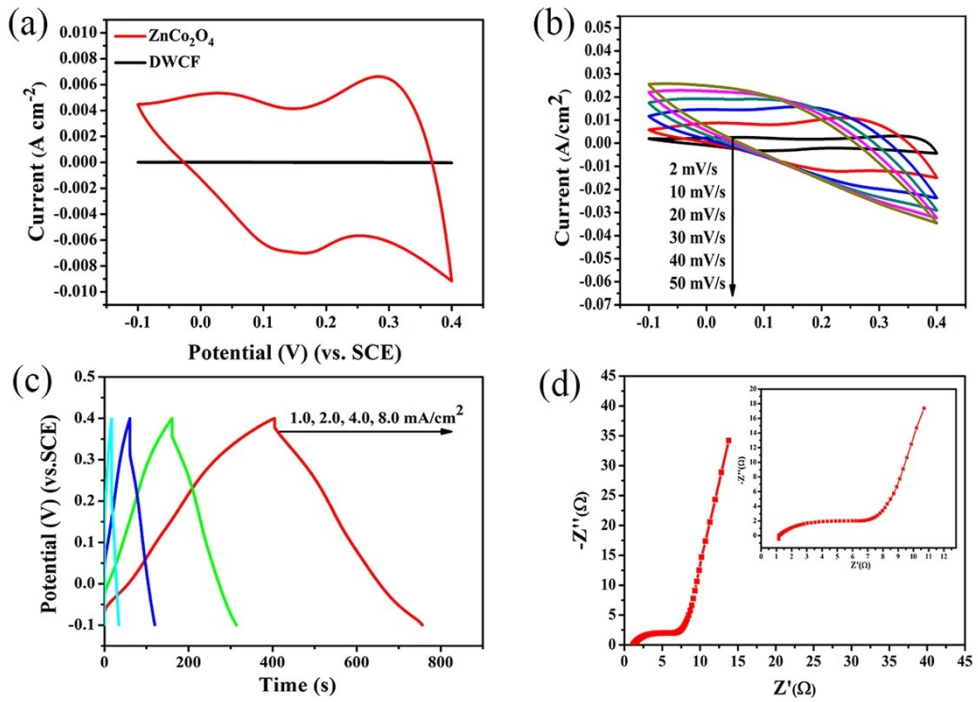

Fig. S2 (a) CV of the positive electrode material in comparison with pristine CNTF electrode. (b) CV curves at different scan rates. (c) GCD curves at different current densities. (d) Nyquist plot.

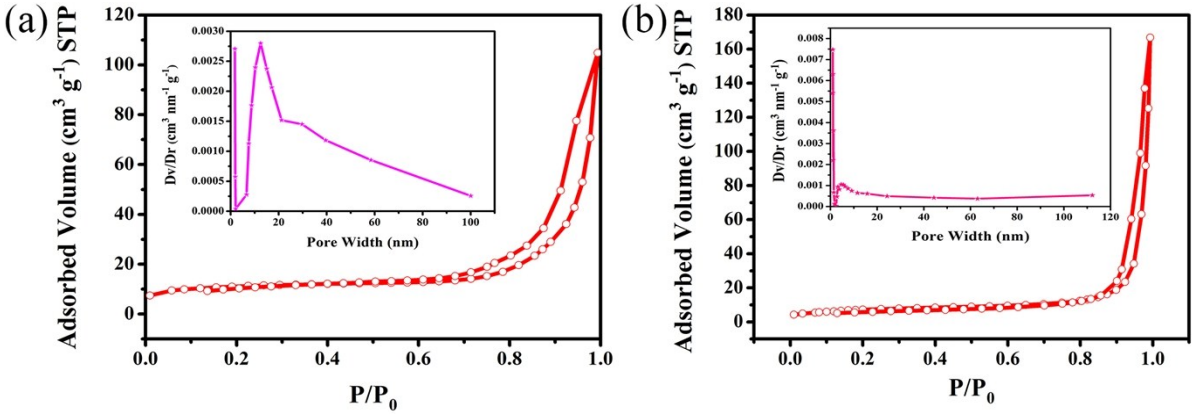

Fig. S3 Nitrogen adsorption/desorption isotherms of (a) cabbage-like $ZnCo_2O_4$ and (b) porous VN nanowires. Inset image is the pore size distribution calculated using a NLDFT model.

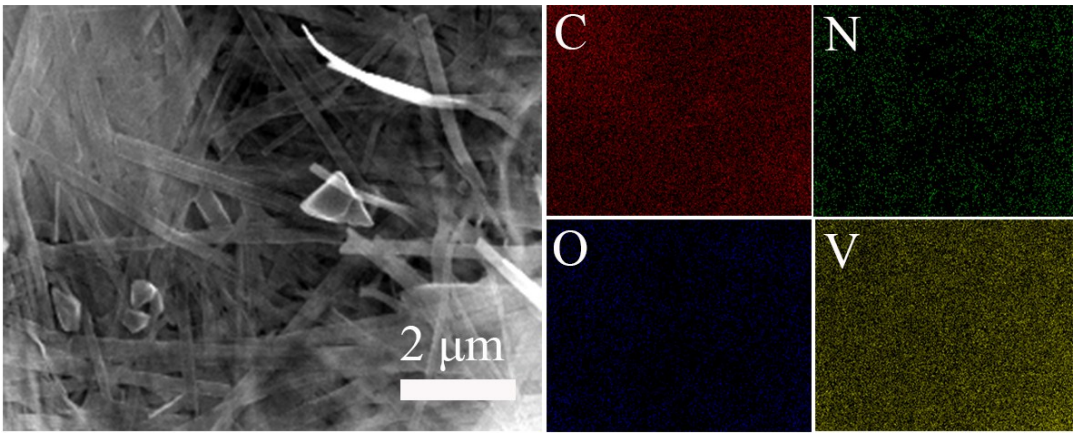

Fig. S4 ESEM image of VN nanowires and EDS mapping images of the C, N, O and V elements.

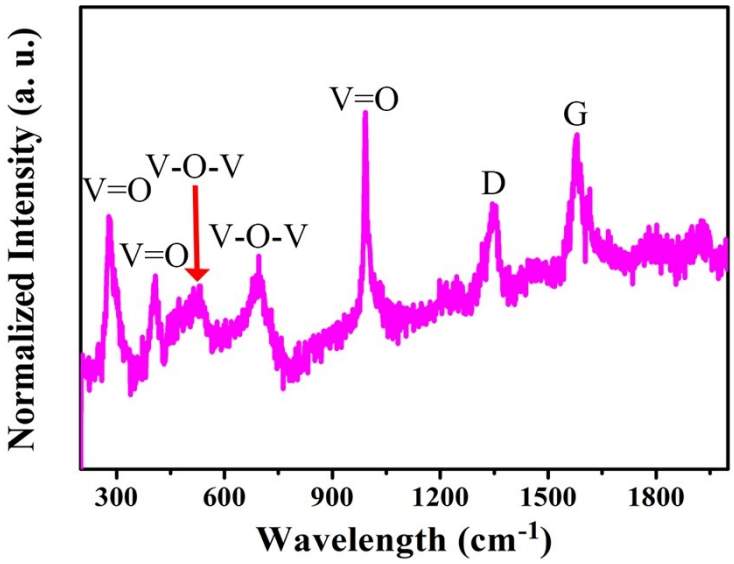

Fig. S5 Raman spectrum of porous VN nanowires. (Raman shift)

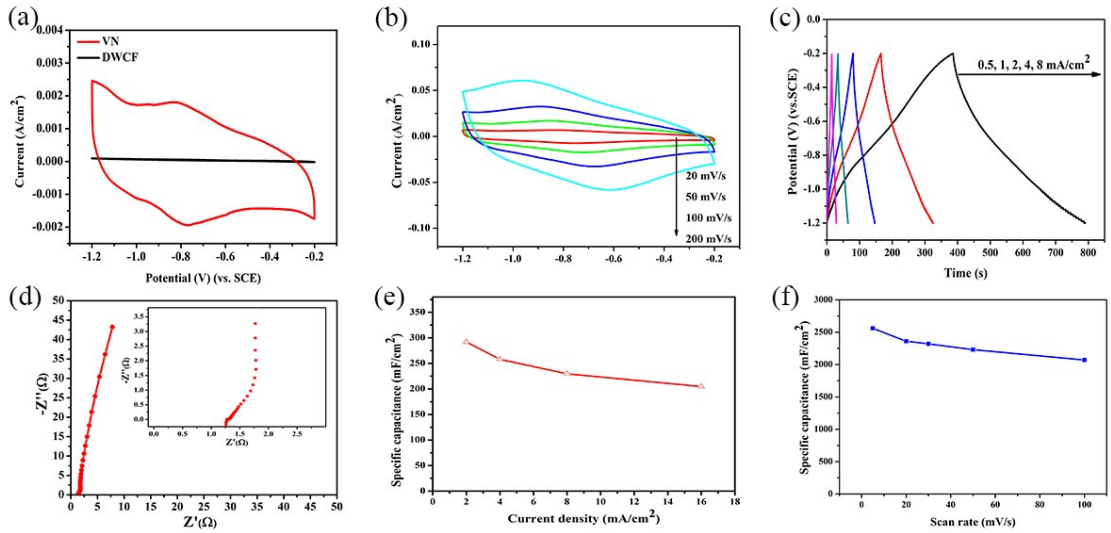

Fig. S6 (a) CV of the negative electrode material in comparison with pristine CNTF electrode. (b) CV curves at different scan rates. (c) GCD curves at different current densities. (d) Nyquist plot. (e) Areal specific capacitance calculated from the charge/discharge curves as a function of current density. (f) Areal specific capacitance vs Scan rate.

The electrochemical properties of the porous VN nanowires/CNTF were investigated using CV, GCD and EIS. Fig. S5a shows the CV of the porous VN nanowires electrode in comparison with the pristine CNTF electrode determined at a scan rate of 20 mV s^{-1}. Comparing to the CV of the VN electrode, the signal from the pristine CNTF electrode was negligible. The CV curves of the porous VN nanowires electrodes taken between -1.2 and -0.2 V in 1 M KOH electrolyte at different scan rates are shown in Fig. S5b. Non-rectangular form of CV curves is due to the pseudocapacitive contribution of VN nanowires. It is attributed to redox reactions of the functional groups (C-O and O-C= O) on the surface of the VN.[1-3] Moreover, no obvious distortion in the CV curves is observed as the sweep rate increases, suggesting a highly reversible system. These excellent CV shapes reveal a very rapid

current response on voltage reversal at each end potential.[4,5] To further understand the high rate capability of the VN, GCD curves were recorded (Fig. S5c), which reveal the relationship between potential (V) and time (t). The shape of the GCD curves shows the characteristic pseudocapacitance, in agreement with the result derived from the CV curves. The maximum specific capacitance is 400 mF cm^{-2} at a current density of 1 mA cm^{-2}. The favorable electrochemical performance of VN can be attributed to the porous structure with a large accessible surface area. It is well-known that the reaction mechanism of an oxide layer is coated on the VN surface in aqueous KOH. The reaction mechanism of VN in KOH electrolyte can be proposed:

$$VN_xO_y + OH^- \leftrightarrow VN_xO_y//OH^- + VN_xO_y\text{-}OH$$

where $VN_xO_y//OH^-$ and $VN_xO_y\text{-}OH$ correspond to the electrical double layer and redox reaction, respectively.

EIS measurements were performed on the VN electrodes in 1 M KOH aqueous electrolyte and Nyquist plot are shown in Fig. S5d. It can be seen that the impedance spectra was composed of one semicircle component at high-frequency and followed by a linear component at the low-frequency. From the point intersecting with the real axis in the range of high frequency, the internal resistance (which is equal to R_b) of the electrode material includes the total resistances of the ionic resistance of the electrolyte, the intrinsic resistance of active material, and the contact resistance at the active material/current collector interface. Owing to the fact that the electrochemical process occurring on the exterior surface of electrodes can be sensed at high frequencies, the semicircle is thought to represent the faradic charge transfer

resistance (R_{ct}) at the interface between the current collector and the VN as well as that within the VN material. Therefore, the semicircle may be due to the faradaic reaction. At the lower frequency, a straight sloping line represents the diffusive resistance (Warburg impendence) of the electrolyte in the electrode pores and the proton diffusion in host material. In addition, the Nyquist plots show a Warburg angle higher than 45°, indicating the suitability of the porous VN nanowires as the electrode materials for supercapacitors.[6] Moreover, the VN electrode embraces excellent rate capability. As shown in Fig. S5e, the reservation rate of VN is up to 71.6% when the discharging current density increases from 2 to 16 mA cm^{-2}. Significantly, the electrode yields the highest areal capacitance of 2600 mF cm^{-2} at the scan rate of 5 mV s^{-1} (Fig. S5f).

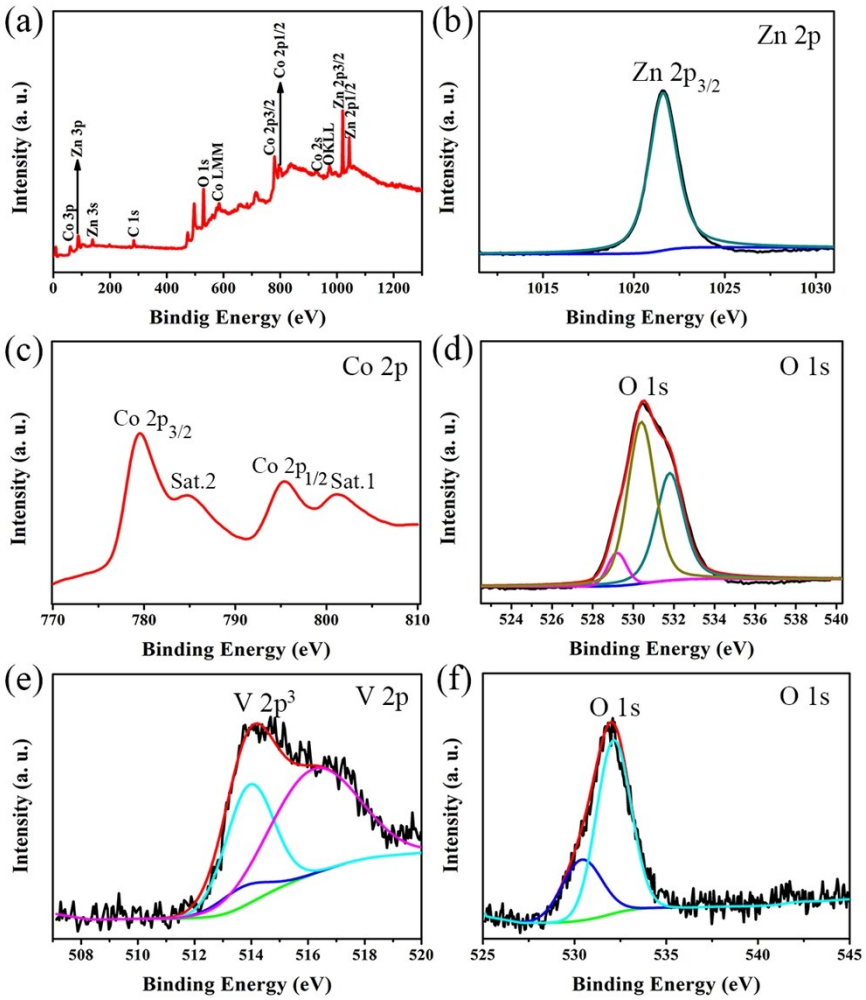

Fig. S7 XPS spectra of cabbage-like $ZnCo_2O_4$ (a) full spectrum and high-resolution spectra of (b) Zn 2p, (c) Co 2p, and (d) O1s. XPS spectra and curve fitting of (e) V $2p^3$ and (f) O 1s of porous VN nanowires.

The XPS general spectrum (Fig. S7a) indicates the presence of Zn, Co and O elements in the Cabbage-like $ZnCo_2O_4$, and C element is derived in the substrate. All of the binding energies in the XPS spectra have been calibrated for specimen charging by referring to C 1s peak (set at 284.6 eV) and no impurity elements were detected. It can be seen from Fig. S7b that the strong peak locates at 1021.6 eV correspond to Zn $2p_{3/2}$ of Zn(II) oxidation state, which is in good accordance with the characteristic peak of Zn^{2+}.[7,8] As shown in Fig. S7c, two major peaks centered at 796.7 and 780.9 eV are

assigned to the Co $2p_{3/2}$ and Co $2p_{1/2}$ peaks, respectively.[9-11] Each peak exhibited a plus 6 V satellite peak at 786.9 (Sat.2) and 802.7 (Sat.1) eV. The position and intensity of Co 2p major and satellite peaks indicate the Co (III) oxidation state.[8,12] The O 1s spectrum (Fig. S7d) can be fitted to three peaks at 529.2, 530.3 and 531.8 eV, which are consistent with the previous reported values.[13] The XPS spectra of porous VN nanowires are exhibited in Fig. S7e and f. Three peaks were required to fit the V $2p^3$ peak from Fig. S7e.[14] The signal at 513.9 eV corresponds to V in VN. In addition, the two other peaks at 514.0 and 516.3 eV are ascribed to the V^{3+} and V^{5+} oxidation states of V in surface oxides. From Fig. S7f, the O 1s can be fitted with two peaks 530.4 and 532.2 eV, which are assigned to oxygen in vanadium oxide and hydroxyl group (-OH) bonded to VN.[14]

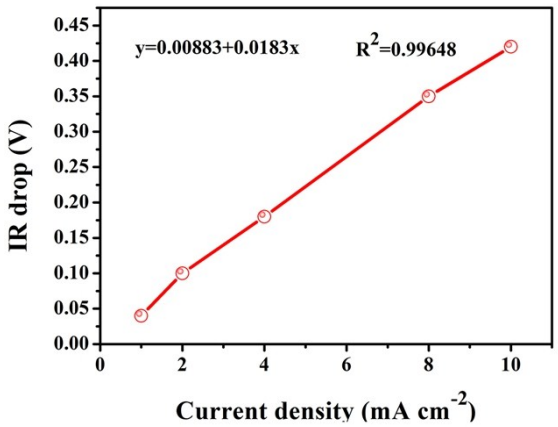

Fig. S8 IR drop as a function of current densities

As well known, the internal resistance has a significant influence on the performance of a device. By plotting the values of initial voltage drop as a function of current density, the internal resistance of the assembled all-solid-state flexible asymmetric supercapacitors device can be presented by the following equation: IR drop (V)=0.00883+0.0183 I (Fig. S8). It indicates that our device has a very small internal resistance, which will be beneficial for high discharge power delivery in practical applications.

1 C. D. Wagner, W. M. Riggs and L. E. Davis, in Handbook of X-ray Photoelectron Spectroscopy (Ed.: J. F. Moulder) Physical Electron- ics Eden Prairie MN 1979.

2 Practical Surface Analysis by Auger and X-ray Photoelectron Spectroscopy (Eds: D. Briggs, M. P. Seah) 2nd ed. Wiley Chichester UK 1983.

3 G. Hopfengaertner, D. Borgmann, I. Rademacher, G. Wedler, E. Hums and G. W. Spitznagel, *J. Electron. Spectrosc.*, 1993, **63,** 91.

4 X. H. Zhou, C. Q. Shang, L. Gu, S.M. Dong, X. Chen, P. X. Han, L. F. Li, J. H. Yao, Z. H. Liu, H. X. Xu, Y. W. Zhu and G. L. Cui, *ACS Appl. Mater. Interfaces*, 2011, **3**, 3058.

5 H. Pang, Q. Y. Lu, Y. C. Li and F. Gao, *Chem. Commun.*, 2009, **48,** 7542.

6 J. Yan, Z. J. Fan, T. Wei, J. Cheng, B. Shao, K. Wang, L. P. Song and M. L. Zhang, *J. Power Sources*, 2009, **194,** 1202.

7 J. M. Xu, L. He, Y. J. Wang, C, J. Zhang and Y. H. Zhang, *Electrochimica Acta*, 2016, **191,** 417.

8 S. G. Mohamed, T. F. Hung, C. J. Chen, C. K. Chen, S. F. Hu, R. S. Liu, K. C. Wang, X. K. Xing, H. M. Liu, A. S. Liu, M. H. Hsieh and B. J. Lee, *Rsc Adv.*, 2013, **3**, 20143.

9 Y. Jin, L. Wang, Y. Shang, J. Gao, J. Li and X. He, *Ionics*, 2015, **10,** 2743.

10 J. Li, J. Wang, D. Wexler, D. Shi, J. Liang, H. Liu, S. Xiong and Y. T. Qian, *J. Mater. Chem. A*, 2013, **1**, 15292.

11 R. Z. Zhao, Q. Li, C. X. Wang and L. W. Yin, *Electrochimica Acta*, 2016, **197**, 58.

12 W. Luo, X. Hu, Y. Sun and Y. Huang, *J. Mater. Chem.*, 201222 (2012) 8916.

13 S. B. Wang, J. Pu, Y. Tong, Y. Y. Cheng, Y. Gao and Z. G. Wang, *J. Mater. Chem. A*, 2014, **2**, 5434.

14 A. M. Glushenkov, D. H. Jurcakova, D. Llewellyn, G. Q. Lu and Y. Chen, *Chem. Mater.*, 2010, **22,** 914.